PEROVSKITES

Bication lead iodide 2D perovskite component to stabilize inorganic α-$CsPbI_3$ perovskite phase for high-efficiency solar cells

Taiyang Zhang,[1] M. Ibrahim Dar,[2] Ge Li,[1] Feng Xu,[1] Nanjie Guo,[1] Michael Grätzel,[2] Yixin Zhao[1]*

Among various all-inorganic halide perovskites exhibiting better stability than organic-inorganic halide perovskites, α-$CsPbI_3$ with the most suitable band gap for tandem solar cell application faces an issue of phase instability under ambient conditions. We discovered that a small amount of two-dimensional (2D) $EDAPbI_4$ perovskite containing the ethylenediamine (EDA) cation stabilizes the α-$CsPbI_3$ to avoid the undesirable formation of the nonperovskite δ phase. Moreover, not only the 2D perovskite of $EDAPbI_4$ facilitate the formation of α-$CsPbI_3$ perovskite films exhibiting high phase stability at room temperature for months and at 100°C for >150 hours but also the α-$CsPbI_3$ perovskite solar cells (PSCs) display highly reproducible efficiency of 11.8%, a record for all-inorganic lead halide PSCs. Therefore, using the bication EDA presents a novel and promising strategy to design all-inorganic lead halide PSCs with high performance and reliability.

INTRODUCTION

In past years, the organic-inorganic hybrid lead halide perovskite solar cells (PSCs) have progressed in an impressive manner approaching commercialization (*1*–*5*). However, the instability of organic-inorganic hybrid perovskite, such as $CH_3NH_3PbI_3$ under thermal stress, might stem from the volatility of the organic cation and has become a challenge for long-term practical deployment. Although organic-inorganic mixed-cation PSCs demonstrating improved efficiency and stabilities have been documented (*6*–*8*), all-inorganic lead halide perovskite absorbers are much desired, specifically because the issues related to the release or decomposition of the organic component can be avoided. The most suitable all-inorganic structure could be based on $CsPbX_3$ perovskite because only the Cs is large enough to occupy the A sites with a suitable tolerance factor to fit the ABX_3 perovskite (B = Pb, X = halide) configuration. The phase-stable $CsPbX_3$ perovskite is usually based on bromide with a suitable tolerance factor, but the $CsPbBr_3$ perovskite has a too wide band gap to realize the fabrication of high-efficiency solar cells. Unfortunately, the α-$CsPbI_3$ perovskite with a band gap of 1.73 eV, which is suitable for tandem solar cells, is structurally unstable and transforms spontaneously into the unwanted δ-$CsPbI_3$ phase under ambient conditions at room temperature. Currently, cesium has been successfully used as A cation along with formamidinium in high-efficiency PSCs, but at concentrations above 20%, it leads to the formation of nonperovskite δ-$CsPbI_3$ (*7*–*12*). Previous reports have suggested that the phase stability of α-$CsPbI_3$ strongly depends on the crystallite size because stability improves by trimming the dimensions of the α-$CsPbI_3$ grains toward the nanoregime (*13*, *14*). Size-dependent phase or thermal stability has been reported in nanomaterials, especially when surfactants were used as growth-controlling agents (*15*, *16*). However, conventional deposition strategies, which do not involve surfactants, mostly yield large-sized $CsPbI_3$ crystallites. Recently, α-$CsPbI_3$ quantum dots with well-controlled size synthesized by hot injection have been fashioned into stable PSCs exhibiting an efficiency of up to 10% (*17*). In addition, a two-dimensional (2D) interface has been demonstrated as an effective strategy to stabilize the organic-inorganic hybrid perovskite or to increase the thermal stability of $CH_3NH_3PbI_3$ (*18*, *19*). However, a 2D segment of these structures may impair the electron transport across the device, lowering their efficiency (*18*). Therefore, it becomes imperative to judiciously design the bication 2D architecture.

Here, we report a new and facile one-step deposition method to obtain highly efficient and stable α-$CsPbI_3$ PSCs (*2*). We stabilize the α-$CsPbI_3$ perovskite films by introducing ethylenediamine cations (EDA^{2+}) whose terminal NH_3^+ groups are expected to cross-link the $CsPbI_3$ perovskite crystal units, rendering them less prone to unwanted phase transition to the δ structure. Stable α-$CsPbI_3$ films have been deposited by introducing a small amount of bication 2D perovskite of $EDAPbI_4$ into the $CsPbI_3$ precursor solution. This cross-links the α-$CsPbI_3$ films without impairing the charge-carrier transport. The resulting α-$CsPbI_3$ structures are highly robust at room temperature for months and can retain their phase even after annealing at 100°C for a week. In addition to the high stability, PSCs based on the α-$CsPbI_3$ films showed highly reproducible photoconversion efficiency (PCE) of 11.8%, a record for α-$CsPbI_3$ devices.

RESULTS

We used a typical one-step method to deposit $CsPbI_3$ films using a regular precursor containing stoichiometric CsI and PbI_2 dissolved in *N*,*N*′-dimethylformamide (DMF). A rough yellowish film was obtained after annealing the precursor film at 150°C. As shown in Fig. 1 (A and B), the absorbance peak located at 414 nm and a strong x-ray diffraction (XRD) peak at 9.78° suggest the formation of the unwanted nonperovskite δ-$CsPbI_3$ phase. This is quite expected because the yellow-to-black phase transformation occurs at 350°C (*13*, *20*). Toward the formation of α-$CsPbI_3$, we develop a low-temperature fabrication method using $PbI_2{\cdot}x$HI ($x > 1.3$) and CsI as precursors. The XRD pattern of $PbI_2{\cdot}x$HI is shown in fig. S1, which exhibits no signature corresponding to the PbI_2 phase and is different from the previous reports on $HPbI_3$ (*21*). The brown perovskite $CsPbI_3$ film was obtained via one-step deposition using the $PbI_2{\cdot}x$HI + CsI precursor, followed by the low-temperature annealing at 100° to 150°C. It seems that the HI in the $PbI_2{\cdot}x$HI adduct decreases the crystallization energy barrier for the α-$CsPbI_3$ phase. The as-prepared film shows an absorbance onset at ~718 nm in Fig. 1A,

[1]School of Environmental Science and Engineering, Shanghai Jiao Tong University, 800 Dongchuan Road, Shanghai 200240, China. [2]Laboratory of Photonics and Interfaces, Institute of Chemical Sciences and Engineering, École Polytechnique Fédérale de Lausanne, CH-1015 Lausanne, Switzerland.
*Corresponding author. Email: yixin.zhao@sjtu.edu.cn

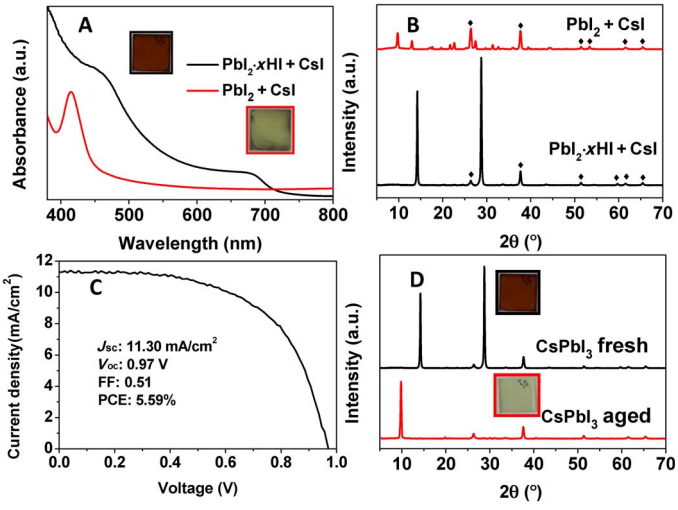

Fig. 1. Spectroscopic and structural characterization, photovoltaic performance, and stability test of $CsPbI_3$ films. (**A**) Ultraviolet-visible (UV-vis) spectra of $CsPbI_3$ films prepared from PbI_2 + CsI and PbI_2·*x*HI + CsI. a.u., arbitrary units. (**B**) XRD patterns of $CsPbI_3$ films prepared from PbI_2 + CsI and PbI_2·*x*HI + CsI. (**C**) Photocurrent density–voltage (*J-V*) curve of α-$CsPbI_3$–based PSCs. FF, fill factor. (**D**) XRD pattern and photos of fresh and aged (within a day) $CsPbI_3$ films prepared from PbI_2·*x*HI + CsI.

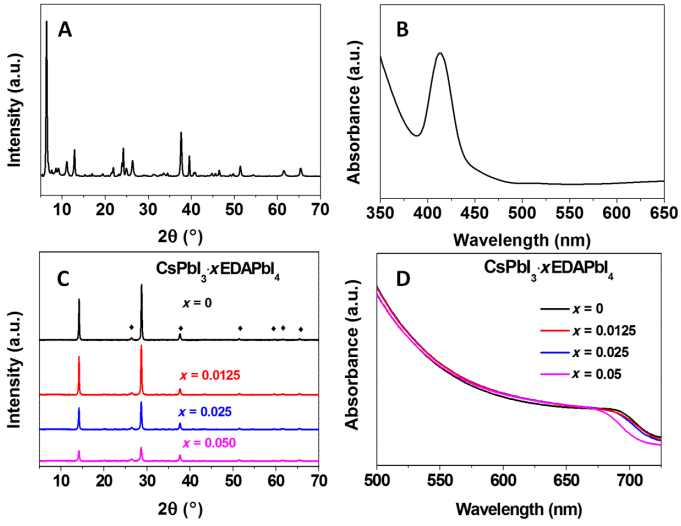

Fig. 2. Structural characterization and spectroscopic study of $EDAPbI_4$ and $CsPbI_3$·*x*$EDAPbI_4$ films. (**A**) XRD pattern and (**B**) UV-vis spectrum of $EDAPbI_4$ films. (**C**) XRD patterns and (**D**) UV-vis absorption spectra of $CsPbI_3$·*x*$EDAPbI_4$ (*x* = 0 to 0.05) perovskites.

indicating a band gap of 1.73 eV, consistent with the previous reports on α-$CsPbI_3$ (*13*, *22*). The XRD pattern (Fig. 1B) obtained from the brown $CsPbI_3$ film could be indexed to a phase-pure cubic α-$CsPbI_3$ perovskite structure (*12*, *13*). However, the PSC based on this α-$CsPbI_3$ film revealed a modest PCE of 5.59% (Fig. 1C), which is comparable to previous reports (*10*, *13*, *23*). Unfortunately, this phase-pure α-$CsPbI_3$ film also suffers from phase instability issues. As shown in Fig. 1D, the brown α-$CsPbI_3$ film transforms into a yellow δ-$CsPbI_3$ film within 12 hours.

In organic-inorganic or inorganic lead halide perovskite, the cation usually occupies one A site in either 3D ABX_3 or 2D A_2BX_4 perovskites. Here, the two NH_3^+ groups of EDA can occupy two A sites and cross-link these 2D layers. This bication 2D perovskite has been theoretically predicted, and the copper halide perovskite based on EDA has been previously reported (*24*–*26*). The $EDAPbI_4$ perovskite film appears greenish, and its absorption spectrum and XRD pattern are listed in Fig. 2. In the XRD pattern (Fig. 2A), a peak located at 2θ = ~6° is a characteristic feature of 2D perovskites (*21*, *27*). Atomic force microscopy (AFM) images reveal that the $EDAPbI_4$ films are consisted of stacks of layered structure (fig. S2). Furthermore, an absorption peak around 420 nm observed in the UV-vis spectrum (Fig. 2B) suggested that the $EDAPbI_4$ is a wider band-gap material (*2*, *28*). Previously, some reports suggested that the bication 2D perovskite can be either a regular (100) layered perovskite or a corrugated (110) layered perovskite (*29*–*33*). Given the band-gap value of $EDAPbI_4$ sample and the short alkyl chain length of the EDA, we assume that it should be the formation of a (110) layered perovskite structure (fig. S3). We introduce a small amount of $EDAPbI_4$ into the $CsPbI_3$ precursor, and these samples are noted as $CsPbI_3$·*x*$EDAPbI_4$. The x-ray photoelectron spectroscopy (XPS) spectra corresponding to an *N* element acquired from the $CsPbI_3$·*x*$EDAPbI_4$ (*x* = 0.0125 to 0.05) samples establish the presence of EDA cations in these films (fig. S4). XRD patterns and UV-vis spectra of $CsPbI_3$·*x*$EDAPbI_4$ samples are listed in Fig. 2 (C and D). Irrespective of their $EDAPbI_4$ content (*x*), all the XRD patterns could be indexed to the standard α-$CsPbI_3$ perovskite phase. No signature (peaks below 2θ = 10°) corresponding to the $EDAPbI_4$ phase was found in the $CsPbI_3$·*x*$EDAPbI_4$ samples, which suggests either the absence of the $EDAPbI_4$ crystal phase or the formation of extremely thin $EDAPbI_4$ layers or crystallites. Amorphous $EDAPbI_4$ could also be present. This matches the behavior of previously reported 2D/3D perovskite formulations (*18*).

Within the detection limit of XRD, no peak indexable to any impurity phase, such as δ-$CsPbI_3$ or PbI_2, is present. The absence of a PbI_2 impurity peak further indicates that ethylenediamine dihydroiodide ($EDAI_2$) is incorporated in the crystal structure. If we add an excess amount (*x*) of PbI_2 without $EDAI_2$ into the precursor, PbI_2 crystallizes as a separate phase (fig. S5). The XRD data indicated that the addition of *x*$EDAPbI_4$ in $CsPbI_3$ does not form a mixture of 2D $EDAPbI_4$ and 3D $CsPbI_3$ perovskite. Furthermore, by increasing the content (*x*) of $EDAPbI_4$ (in $CsPbI_3$·*x*$EDAPbI_4$ samples), the intensity of the XRD peaks decreases, whereas their peak width broadens, indicating the decrease of crystallite size. Such a confinement effect was further manifested by the blueshift of absorption onset (Fig. 2D), which is quite evident for the $CsPbI_3$·0.05$EDAPbI_4$ sample. The photoluminescence (PL) spectra of $CsPbI_3$·*x*$EDAPbI_4$ samples (fig. S6A) also exhibited blueshift when the content of $EDAPbI_4$ is increased. Moreover, their PL lifetimes also increased with the content of $EDAPbI_4$ (fig. S5B). Such a blueshift has been observed in $CsPbI_3$ quantum dots synthesized using hot-injection solution-based method and other hybrid lead halide perovskite films with the incorporation of 2D perovskite (*34*). The blueshift in both UV-vis and PL spectra can be ascribed either to the formation of 2D/3D perovskite of $CsPbI_3$·0.05$EDAPbI_4$ or to the decrease in crystal size. In the plausible 2D/3D configuration, we hypothesize that the (110) layered 2D $EDAPbI_4$ component can also function as an interface to separate small $CsPbI_3$ crystal units, as in the regular 2D/3D perovskite. The 2D $EDAPbI_4$ might also work as a blocking layer similar to the surfactant, which can eventually reduce the crystallite size of the $CsPbI_3$·*x*$EDAPbI_4$ perovskite structures. Previous reports have suggested that the reduced crystal size can lead to the blueshift of optical spectrum even when the crystal size is larger than the Bohr radius (*35*).

Furthermore, the addition of a small amount of $EDAPbI_4$ also helps reduce the pinholes in the deposited $CsPbI_3$ perovskite films and passivates their surface, similar to a previously reported regular 2D/3D or cross-linked 2D/3D perovskite (*18*, *28*). Figure S6B shows that the PL lifetime of the $CsPbI_3{\cdot}xEDAPbI_4$ film increases with its $EDAPbI_4$ content, suggesting a suppression of radiation-less recombination. The scanning electron microscopy (SEM) and AFM images (Fig. 3, A and B) show that the grain size of $CsPbI_3{\cdot}xEDAPbI_4$ decreases markedly from ~300 nm ($x = 0$) to ~35 nm ($x = 0.025$) with increasing $EDAPbI_4$ content. This is consistent with the XRD peak broadening observed in Fig. 2. Note that the pinholes became much less with the addition of $EDAPbI_4$, which is favorable for high-performance PSC fabrication.

All these results reveal that the addition of a small content of $EDAPbI_4$ has strongly affected the properties of $CsPbI_3$. To rationalize this observation, we first exclude the possibility of Cs^+ substitution by EDA on a single A site of $CsPbI_3$ to form an $EDA_xCs_{1-2x}PbI_3$ mixed-cation perovskites on the basis of the large size of EDA ($r = 0.31$ nm). Moreover, replacing Cs^+ by larger cations, such as EDA, should narrow the band gap and induce an XRD peak shift, although we observe a widening of the band gap and no shift in the XRD peak position.

We adopted a planar configuration to fabricate PSCs based on these $CsPbI_3{\cdot}xEDAPbI_4$ perovskites. The photovoltaic parameters extracted from the *J-V* curves (Fig. 4A) are listed in Table 1. We found that $CsPbI_3{\cdot}xEDAPbI_4$ (x = 0.0125 to 0.05) devices show a much better performance than those based on the pure $CsPbI_3$. The enhancement in all the photovoltaic parameters, that is, J_{SC}, V_{OC}, and FF, can be attributed to less pinholes, desired charge-carrier dynamics, and surface passivation by $EDAPbI_4$. For $x \leq 0.025$, the transient photovoltage decay curves (fig. S7) exhibit monotonic increase in the lifetime with the $EDAPbI_4$ incorporation, which is consistent with the PL decay dynamics (fig. S6B). Furthermore, the 2D $EDAPbI_4$ in these $CsPbI_3{\cdot}xEDAPbI_4$ (x = 0.0125 to 0.05) compositions seem to have less impact on the charge transfer because this can be significantly hindered in regular 2D/3D PSCs (*18*). The best performing cell used the $CsPbI_3{\cdot}0.025EDAPbI_4$ perovskite formulation showing a remarkable PCE of 11.8% under reverse scan. To the best of our knowledge, this is a record for $CsPbI_3$-based PSCs. Hysteresis between different scan directions is also found in our planar cell structure (fig. S8), and the scan rate–independent maximum power tracking (Fig. 4B) indicates an efficiency of 10.5%. The integrated J_{SC} obtained from the incident photon-to-electron conversion efficiency (IPCE) is consistent with the values extracted from the *J-V* curves. Note that the IPCE value of the champion cell has reached 86% over a wide wavelength range. Device performance was also highly reproducible, as shown in Fig. 4D. The improved reproducibility demonstrated by the $CsPbI_3{\cdot}xEDAPbI_4$ solar cells can be ascribed to the better control on the film formation (less pinholes) (*36*, *37*).

The best solar cell based on the $CsPbI_3{\cdot}0.025EDAPbI_4$ perovskite showed good stability because it retained ~10% efficiency after storing in a dark dry box for 1 month without any encapsulation (Fig. 5A). All the above results establish that the formation of $CsPbI_3{\cdot}0.025EDAPbI_4$ perovskite significantly improves the performance of the devices. Besides the high efficiency, the thermal stability of $CsPbI_3{\cdot}xEDAPbI_4$ films markedly improved as compared to the pure $CsPbI_3$ (fig. S9). The α-$CsPbI_3$ perovskite phase of the $CsPbI_3{\cdot}0.025EDAPbI_4$ sample can be retained for months at room temperature (fig. S10) and after heating the $CsPbI_3{\cdot}0.025EDAPbI_4$ film at 100°C for 1 week, as shown in Fig. 5B.

DISCUSSION

All of the above results demonstrate the superior photovoltaic performance of $CsPbI_3{\cdot}xEDAPbI_4$ over pure α-$CsPbI_3$–based PSCs. It appears that the hypothesized $EDAPbI_4$ 2D perovskite component not only stabilizes the α-$CsPbI_3$ perovskite phase but also reduces the deterioration of charge-carrier transport across the perovskite film caused by the "insulating" long alkyl spacing layers (*18*, *38*). This improvement in both efficiency and stability is closely related to this unique bifunctional cation perovskite component. We cannot obtain the efficient and stable α-$CsPbI_3$ perovskite films if we merely add $EDAI_2$ instead of $EDAI_2$ + PbI_2 into the $CsPbI_3$ precursor solution. In addition, if the EDA is replaced by the monofunctional ethylamine (EA) in the regular 2D/3D $CsPbI_3{\cdot}xEA_2PbI_4$ samples, the perovskite phase of $CsPbI_3{\cdot}xEA_2PbI_4$ ($x = 0.025$) deteriorated as markedly as observed in the pure $CsPbI_3$. As shown in fig. S11, the typical sample of brown $CsPbI_3{\cdot}0.025EA_2PbI_4$ turns into a yellow phase within a day at room temperature. In contrast, the bication EDA with CH_2–CH_2 can effectively assemble the $CsPbI_3$ crystal units. Furthermore, all the $CsPbI_3{\cdot}xEA_2PbI_4$ perovskite film–based solar cells exhibited poor photovoltaic performance, and the best *J-V* curve obtained from the PSCs based on $CsPbI_3{\cdot}0.025EA_2PbI_4$ is listed in fig. S12. The efficiency is only ~4.4%, which is way too low than that of $CsPbI_3$ PSCs. Such low stability could be due to either the weak

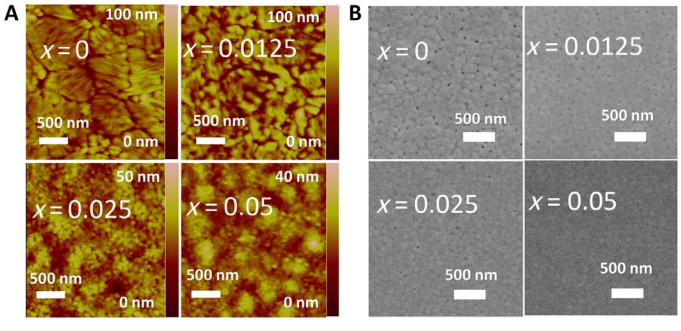

Fig. 3. Effect of $EDAPbI_4$ on the evolution of morphology of $CsPbI_3{\cdot}xEDAPbI_4$. (**A**) AFM and (**B**) SEM images of perovskite films obtained from the $CsPbI_3{\cdot}xEDAPbI_4$ additive precursor (x = 0, 0.0125, 0.025, and 0.05).

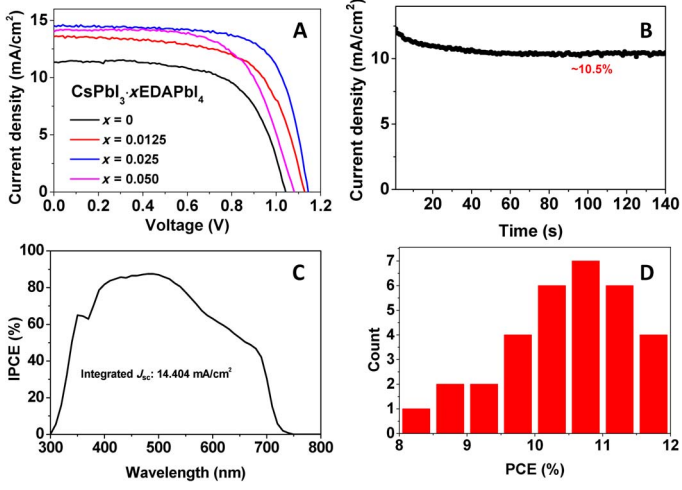

Fig. 4. Device characteristics for $CsPbI_3{\cdot}xEDAPbI_4$ films. (**A**) Typical *J-V* curves of $CsPbI_3{\cdot}xEDAPbI_4$ PSCs. (**B**) Stable current output at the maximum point of the champion $CsPbI_3{\cdot}0.025EDAPbI_4$ PSC. (**C**) IPCE of the best solar cell based on the $CsPbI_3{\cdot}0.025EDAPbI_4$ perovskite. (**D**) Histogram of device efficiencies of $CsPbI_3{\cdot}0.025EDAPbI_4$ PSCs based on 32 cells from three batches.

Table 1. Effect of $EDAPbI_4$ on the metrics of planar $CsPbI_3$ PSCs (12 to 32 cells for each type).

Precursor type	J_{SC} (mA/cm^2)	V_{OC} (V)	FF	η (%)
Pure $CsPbI_3$	11.33 (11.63 ± 1.55)	1.04 (0.89 ± 0.09)	0.65 (0.53 ± 0.06)	7.66 (5.56 ± 1.16)
$CsPbI_3$·0.0125$EDAPbI_4$	13.59 (13.31 ± 0.36)	1.13 (1.09 ± 0.06)	0.65 (0.56 ± 0.06)	9.98 (8.22 ± 1.46)
$CsPbI_3$·0.025$EDAPbI_4$	14.53 (14.05 ± 0.57)	1.15 (1.13 ± 0.02)	0.71 (0.64 ± 0.08)	11.86 (10.42 ± 0.91)
$CsPbI_3$·0.05$EDAPbI_4$	13.97 (13.17 ± 0.88)	1.08 (1.06 ± 0.03)	0.65 (0.61 ± 0.02)	9.81 (8.58 ± 0.66)

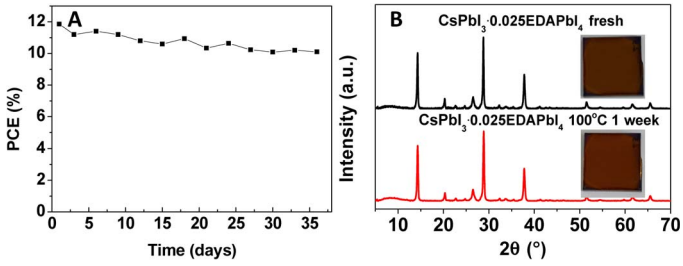

Fig. 5. Stability test of $CsPbI_3$·0.025$EDAPbI_4$-based devices and films. (**A**) PCE of the champion PSC fabricated from $CsPbI_3$·0.025$EDAPbI_4$ as a function of storage time in a dark dry box. (**B**) XRD pattern and images of the $CsPbI_3$·0.025$EDAPbI_4$ film heated at 100°C in a dry box for 1 week.

steric effect of short alkyl chain containing the EA cation compared to EDA or the lack of bication effect. Not appropriately, we used a longer-chain alkylamine, such as butylamine (BA), with an even larger size to form the $CsPbI_3$·0.025BA_2PbI_4 perovskite. The $CsPbI_3$·0.025BA_2PbI_4 samples show some improved stability than those of $CsPbI_3$·0.025EA_2PbI_4 but still far more unstable than the $CsPbI_3$·0.025$EDAPbI_4$ samples (fig. S13). This result suggested that both the steric effect and bication in the 2D perovskite improve the phase stability, although the latter might be more important.

To further understand the mechanism behind the high phase stability of $CsPbI_3$·$x$$EDAPbI_4$, we used other two bications, that is, 1,4-diaminobutane (BDA^{2+}) and 2,2′-(ethylenedioxy)bis(ethylammonium) ($EDBE^{2+}$), which are similar to EDA. The $BDAPbI_4$ perovskite has been demonstrated to be a (100) layered bication 2D perovskite, whereas the $EDBEPbI_4$ has been shown to be a (110) layered 2D perovskite (*29*–*31*, *33*). Like $CsPbI_3$·0.025$EDAPbI_4$, the $CsPbI_3$·0.025$BDAPbI_4$ samples are composed of smaller perovskite crystallites (fig. S14), exhibiting significantly enhanced thermal stability than pristine $CsPbI_3$. However, after holding at 100°C for 3 days, the $CsPbI_3$·0.025$EDAPbI_4$ film turns into the yellow δ phase, suggesting that its phase stability is lower than that of $CsPbI_3$·0.025$EDAPbI_4$ (fig. S15A). The main difference between $EDAPbI_4$ and $BDAPbI_4$ is that the former is a (110) layered 2D perovskite, whereas the latter is a (100) layered 2D perovskite. It is likely that the higher phase stability of $CsPbI_3$·0.025$EDAPbI_4$ could be ascribed to the unique (110) layered perovskite structure of $EDAPbI_4$. The $CsPbI_3$·0.025$EDBEPbI_4$ sample with the (110) layered $EDBEPbI_4$ shows enhanced thermal stability than $CsPbI_3$; however, as compared to $CsPbI_3$·0.025$BDAPbI_4$, its thermal stability is even poorer, as shown in fig. S15B. It is found that the $CsPbI_3$·0.025$EDBEPbI_4$ perovskite sample shows a larger crystal size than $CsPbI_3$·0.025$BDAPbI_4$ and $CsPbI_3$·0.025$EDAPbI_4$, suggesting that the lower thermal stability of $CsPbI_3$·0.025$EDBEPbI_4$ sample might be due to the presence of large crystallites. All these findings demonstrate that the confluence of reduced crystal size and the unique (110) layered bication 2D perovskite structure enhance the overall phase stability of α-$CsPbI_3$. Specifically, we ascribe the enhanced phase stability of $CsPbI_3$·$x$$EDAPbI_4$ to the reduced crystallite size and the $EDAPbI_4$ component's unique (110) layered structure.

In summary, we report a phase-stable α-$CsPbI_3$ film with an $EDAPbI_4$ 2D perovskite component prepared via a novel and facile single-step method under ambient conditions for high-efficiency all-inorganic PSCs. By introducing the 2D perovskite of $EDAPbI_4$, the structurally robust α-$CsPbI_3$ perovskite films were obtained even at temperatures several hundred°C below the phase transition point. The addition of a small amount of $EDAPbI_4$ stabilizes the α-$CsPbI_3$. Moreover, these perovskite films can retain the α-$CsPbI_3$ phase even after annealing at 100°C for >150 hours and are also stable at room temperature for months. The $EDAPbI_4$ (x = 0 to 0.05) not only enhances the phase stability of α-$CsPbI_3$ crystallites significantly but also connects them for effective electron transfer and passivates the surface defects. Finally, a champion α-$CsPbI_3$ PSC based on $CsPbI_3$·0.025$EDAPbI_4$ perovskite films showing a PCE of 11.8%, a record for all-inorganic PSCs, was realized. Therefore, the concept of using bication presents a novel and promising strategy for designing all-inorganic lead halide PSCs yielding high performance and reliability. Such a bication 2D perovskite with different oriented layer structure concepts could also be extended to balance high performance and high stability in organic-inorganic hybrid lead halide perovskites with the incorporation of a 2D component for their use in optoelectronic applications.

MATERIALS AND METHODS

Materials

$EDAI_2$ was synthesized by reacting EDA and hydroiodic acid with a molar ratio of 1:2.2 in an ice bath for 2 hours. The precipitate was collected by rotary evaporation, washed three times with diethyl ether, and then vacuum-dried. 1,4-Diaminobutane dihydroiodide ($BDAI_2$), 2,2′-(ethylenedioxy)bis(ethylammonium) dihydroiodide ($EDBEI_2$), ethylammonium iodide (EAI), and butylammonium iodide (BAI) were synthesized following the similar procedure. The PbI_2·xHI sample was synthesized as follows: 1 M PbI_2 in DMF solution was reacted with 1.5 molar ratio of hydroiodic acid for 1 hour, followed by rotary evaporation, washed three times with diethyl ether, and then vacuum-dried; the concentration of PbI_2 in the final product should be within the range of 62 to 65 weight %. All the other materials were purchased from Sigma-Aldrich and used as received without any purification.

The $CsPbI_3$·$x$$EDAPbI_4$ precursor solution was prepared by dissolving 1 mmol of PbI_2·xHI and 1 mmol of CsI (1 mM) in 2 ml of DMF to form a 0.5 M precursor solution mixed with different x ratios of

0.5 M $EDAPbI_4$ solution. The 0.5 M $EDAPbI_4$ solution was obtained by dissolving 0.5 mmol of $EDAI_2$ and 0.5 mmol of PbI_2 into 1 ml of DMF.

Device fabrication

A 20-nm-thick compact TiO_2 layer was first deposited on the patterned fluorine-doped tin oxide using 0.2 M Ti(IV) bis(ethyl acetoacetato) diisopropoxide in 1-butanol solution at 450°C, followed by annealing at 450°C for 1 hour. The $CsPbI_3{\cdot}xEDAI_2$ precursor solutions were then spin-coated onto the prewarmed *c*-TiO_2–coated substrate (50°C) at 3500 rpm for 30 s, followed by annealing at 150°C for 2 min. After the films were cooled down to room temperature, a layer of hole transport material of 0.1 M spiro-MeOTAD, 0.035 M bis(trifluoromethane)sulfonimide lithium salt, and 0.12 M 4-*tert*-butylpyridine in chlorobenzene/acetonitrile (10:1, v/v) solution was spin-coated at 4000 rpm for 20 s. Finally, a 100-nm-thick Ag contact layer was thermally evaporated as back contact.

Characterization

The crystal structures of the $CsPbI_3{\cdot}xEDAPbI_4$ films were examined by a Shimadzu XRD-6100 diffractometer with Cu K_α radiation. The morphologies of the $CsPbI_3{\cdot}xEDAPbI_4$ films were observed by a JSM-7800F Prime SEM and a Bruker Multimode Nanoscope IIIa AFM. The absorption spectra of the $EDAPbI_4$ and $CsPbI_3{\cdot}xEDAPbI_4$ perovskite films were taken on a Cary 60 UV-vis spectrophotometer. XPS spectra were acquired with a Kratos Axis Ultra DLD spectrometer (Kratos Analytical-A Shimadzu Group Company) using a monochromatic Al K source (1486.6 eV). Time-integrated PL and time-resolved PL experiments were performed by exciting the samples deposited onto a nonconducting glass using the second harmonic of a picosecond mode–locked Ti-sapphire laser (80.5 MHz) at 420 nm under ambient conditions. The average power was kept around 0.05 $\mu J/cm^2$ per pulse. Using a 32-cm focal length monochromator equipped with a charge-coupled device, which has a spectral resolution of >1 meV, and a streak camera with a temporal resolution of >2 ps, the PL data were spectrally and temporally analyzed. The *J-V* curves of the PSCs were measured by a Keithley 2401 SourceMeter under simulated air mass 1.5-global illumination with a scan rate of 0.05 V/S (100 mW/cm^2) (Enlitech SS-F5-3A Class AAA Solar Simulator; the light intensity was calibrated by a stand Si cell before test), equipped with a nonreflective metal mask with an aperture area of 0.12 cm^2; the IPCE was measured on a QE-3011 system from Enlitech. All the *J-V* and IPCE tests were processed in atmosphere with a relative humidity of 30 to 45%.

SUPPLEMENTARY MATERIALS

Supplementary material for this article is available at http://advances.sciencemag.org/cgi/content/full/3/9/e1700841/DC1

fig. S1. Comparative analysis of crystal structures of $PbI_2{\cdot}xHI$ and $HPbI_3$.
fig. S2. Morphology of $EDAPbI_4$ films.
fig. S3. Schematic structure of (110) layered 2D films.
fig. S4. The organic compositions of $CsPbI_3{\cdot}xEDAPbI_4$ films.
fig. S5. Characterization of $CsPbI_3$ + 0.05PbI_2 with or without $EDAI_2$.
fig. S6. Effect of $EDAPbI_4$ on the optical properties.
fig. S7. Effect of $EDAPbI_4$ on the transient photovoltage behavior.
fig. S8. Hysteresis behavior of $CsPbI_3{\cdot}0.025EDAPbI_4$-based device.
fig. S9. Effect of $EDAPbI_4$ on the phase stability of $CsPbI_3{\cdot}xEDAPbI_4$ perovskite films.
fig. S10. Phase stability of $CsPbI_3{\cdot}0.025EDAPbI_4$ perovskite film under room temperature.
fig. S11. Phase stability of $CsPbI_3{\cdot}0.025EA_2PbI_4$-based films.
fig. S12. Device performance of $CsPbI_3{\cdot}0.025EA_2PbI_4$-based solar cell.
fig. S13. Phase stability of $CsPbI_3{\cdot}0.025BA_2PbI_4$-based films.
fig. S14. Effect of $CsPbI_3{\cdot}0.025BDAPbI_4$ and $CsPbI_3{\cdot}0.025EDBEPbI_4$ 2D perovskite component on the evolution of morphology.
fig. S15. Phase stability of $CsPbI_3{\cdot}0.025BDAPbI_4$ and $CsPbI_3{\cdot}0.025EDBEPbI_4$ films.

REFERENCES AND NOTES

1. N.-G. Park, M. Grätzel, T. Miyasaka, K. Zhu, K. Emery, Towards stable and commercially available perovskite solar cells. *Nat. Energy* **1**, 16152 (2016).
2. Y. Zhao, K. Zhu, Organic–inorganic hybrid lead halide perovskites for optoelectronic and electronic applications. *Chem. Soc. Rev.* **45**, 655–689 (2016).
3. A. Kojima, K. Teshima, Y. Shirai, T. Miyasaka, Organometal halide perovskites as visible-light sensitizers for photovoltaic cells. *J. Am. Chem. Soc.* **131**, 6050–6051 (2009).
4. H.-S. Kim, C.-R. Lee, J.-H. Im, K.-B. Lee, T. Moehl, A. Marchioro, S.-J. Moon, R. Humphry-Baker, J.-H. Yum, J. E. Moser, M. Grätzel, N.-G. Park, Lead iodide perovskite sensitized all-solid-state submicron thin film mesoscopic solar cell with efficiency exceeding 9%. *Sci. Rep.* **2**, 591 (2012).
5. M. M. Lee, J. Teuscher, T. Miyasaka, T. N. Murakami, H. J. Snaith, Efficient hybrid solar cells based on meso-superstructured organometal halide perovskites. *Science* **338**, 643–647 (2012).
6. M. Saliba, T. Matsui, K. Domanski, J.-Y. Seo, A. Ummadisingu, S. M. Zakeeruddin, J.-P. Correa-Baena, W. R. Tress, A. Abate, A. Hagfeldt, M. Grätzel, Incorporation of rubidium cations into perovskite solar cells improves photovoltaic performance. *Science* **354**, 206–209 (2016).
7. D. P. McMeekin, G. Sadoughi, W. Rehman, G. E. Eperon, M. Saliba, M. T. Hörantner, A. Haghighirad, N. Sakai, L. Korte, B. Rech, M. B. Johnston, L. M. Herz, H. J. Snaith, A mixed-cation lead mixed-halide perovskite absorber for tandem solar cells. *Science* **351**, 151–155 (2016).
8. M. Saliba, T. Matsui, J.-Y. Seo, K. Domanski, J.-P. Correa-Baena, M. K. Nazeeruddin, S. M. Zakeeruddin, W. Tress, A. Abate, A. Hagfeldt, M. Grätzel, Cesium-containing triple cation perovskite solar cells: Improved stability, reproducibility and high efficiency. *Energy Environ. Sci.* **9**, 1989–1997 (2016).
9. C. Yi, J. Luo, S. Meloni, A. Boziki, N. Ashari-Astani, C. Grätzel, S. M. Zakeeruddin, U. Röthlisberger, M. Grätzel, Entropic stabilization of mixed A-cation ABX_3 metal halide perovskites for high performance perovskite solar cells. *Energy Environ. Sci.* **9**, 656–662 (2016).
10. H. Choi, J. Jeong, H.-B. Kim, S. Kim, B. Walker, G.-H. Kim, J. Young Kim, Cesium-doped methylammonium lead iodide perovskite light absorber for hybrid solar cells. *Nano Energy* **7**, 80–85 (2014).
11. J.-W. Lee, D.-H. Kim, H.-S. Kim, S.-W. Seo, S. M. Cho, N.-G. Park, Formamidinium and cesium hybridization for photo- and moisture-stable perovskite solar cell. *Adv. Energy Mater.* **5**, 1501310 (2015).
12. Z. Li, M. Yang, J.-S. Park, S.-H. Wei, J. J. Berry, K. Zhu, Stabilizing perovskite structures by tuning tolerance factor: Formation of formamidinium and cesium lead iodide solid-state alloys. *Chem. Mater.* **28**, 284–292 (2016).
13. G. E. Eperon, G. M. Paterno, R. J. Sutton, A. Zampetti, A.-A. Haghighirad, F. Cacialli, H. J. Snaith, Inorganic caesium lead iodide perovskite solar cells. *J. Mater. Chem. A* **3**, 19688–19695 (2015).
14. L. Protesescu, S. Yakunin, M. I. Bodnarchuk, F. Krieg, R. Caputo, C. H. Hendon, R. X. Yang, A. Walsh, M. V. Kovalenko, Nanocrystals of cesium lead halide perovskites ($CsPbX_3$, X = Cl, Br, and I): Novel optoelectronic materials showing bright emission with wide color gamut. *Nano Lett.* **15**, 3692–3696 (2015).
15. C. Burda, X. Chen, R. Narayanan, M. A. El-Sayed, Chemistry and properties of nanocrystals of different shapes. *Chem. Rev.* **105**, 1025–1102 (2005).
16. Y. Fu, T. Wu, J. Wang, J. Zhai, M. J. Shearer, Y. Zhao, R. J. Hamers, E. Kan, K. Deng, X.-Y. Zhu, S. Jin, Stabilization of the metastable lead iodide perovskite phase via surface functionalization. *Nano Lett.* **17**, 4405–4414 (2017).
17. A. Swarnkar, A. R. Marshall, E. M. Sanehira, B. D. Chernomordik, D. T. Moore, J. A. Christians, T. Chakrabarti, J. M. Luther, Quantum dot–induced phase stabilization of α-$CsPbI_3$ perovskite for high-efficiency photovoltaics. *Science* **354**, 92–95 (2016).
18. H. Tsai, W. Nie, J.-C. Blancon, C. C. Stoumpos, R. Asadpour, B. Harutyunyan, A. J. Neukirch, R. Verduzco, J. J. Crochet, S. Tretiak, L. Pedesseau, J. Even, M. A. Alam, G. Gupta, J. Lou, P. M. Ajayan, M. J. Bedzyk, M. G. Kanatzidis, A. D. Mohite, High-efficiency two-dimensional Ruddlesden–Popper perovskite solar cells. *Nature* **536**, 312–316 (2016).
19. N. Wang, L. Cheng, R. Ge, S. Zhang, Y. Miao, W. Zou, C. Yi, Y. Sun, Y. Cao, R. Yang, Y. Wei, Q. Guo, Y. Ke, M. Yu, Y. Jin, Y. Liu, Q. Ding, D. Di, L. Yang, G. Xing, H. Tian, C. Jin, F. Gao, R. H. Friend, J. Wang, W. Huang, Perovskite light-emitting diodes based on solution-processed self-organized multiple quantum wells. *Nat. Photonics* **10**, 699–704 (2016).
20. C. C. Stoumpos, C. D. Malliakas, M. G. Kanatzidis, Semiconducting tin and lead iodide perovskites with organic cations: Phase transitions, high mobilities, and near-infrared photoluminescent properties. *Inorg. Chem.* **52**, 9019–9038 (2013).
21. F. Wang, H. Yu, H. Xu, N. Zhao, $HPbI_3$: A new precursor compound for highly efficient solution-processed perovskite solar cells. *Adv. Funct. Mater.* **25**, 1120–1126 (2015).
22. G. E. Eperon, S. D. Stranks, C. Menelaou, M. B. Johnston, L. M. Herz, H. J. Snaith, Formamidinium lead trihalide: A broadly tunable perovskite for efficient planar heterojunction solar cells. *Energy Environ. Sci.* **7**, 982–988 (2014).
23. T. S. Ripolles, K. Nishinaka, Y. Ogomi, Y. Miyata, S. Hayase, Efficiency enhancement by changing perovskite crystal phase and adding a charge extraction interlayer in organic

amine free-perovskite solar cells based on cesium. *Sol. Energy Mater. Sol. Cells* **144**, 532–536 (2016).
24. C. Li, F. A. Evangelista, Towards numerically robust multireference theories: The driven similarity renormalization group truncated to one- and two-body operators. *J. Chem. Phys.* **144**, 164114 (2016).
25. H. Arend, W. Huber, F. H. Mischgofsky, G. K. Richter-Van Leeuwen, Layer perovskites of the $(C_nH_{2n+1}NH_3)_2MX_4$ and $NH_3(CH_2)_mNH_3MX_4$ families with *M* = *Cd*, *Cu*, *Fe*, *Mn* or *Pd* and *X* = *Cl* or *Br*: Importance, solubilities and simple growth techniques. *J. Cryst. Growth* **43**, 213–223 (1978).
26. S. Skaarup, R. W. Berg, Structural properties and vibrational spectra of the ethylene-diammonium family of perovskite layer-type crystals: $[NH_3CH_2CH_2NH_3]$ $[MCl_4]$, *M* = Ni, Pd, Cu, Cd, Mn. *J. Solid State Chem.* **26**, 59–67 (1978).
27. Z. Cheng, J. Lin, Layered organic–inorganic hybrid perovskites: Structure, optical properties, film preparation, patterning and templating engineering. *CrstEngComm* **12**, 2646–2662 (2010).
28. G. Li, T. Zhang, N. Guo, F. Xu, X. Qian, Y. Zhao, Ion-exchange-induced 2D–3D conversion of $HMA_{1-x}FA_xPbI_3Cl$ perovskite into a high-quality $MA_{1-x}FA_xPbI_3$ perovskite. *Angew. Chem. Int. Ed.* **55**, 13460–13464 (2016).
29. D. Cortecchia, S. Neutzner, A. R. Srimath Kandada, E. Mosconi, D. Meggiolaro, F. De Angelis, C. Soci, A. Petrozza, Broadband emission in two-dimensional hybrid perovskites: The role of structural deformation. *J. Am. Chem. Soc.* **139**, 39–42 (2017).
30. E. R. Dohner, E. T. Hoke, H. I. Karunadasa, Self-assembly of broadband white-light emitters. *J. Am. Chem. Soc.* **136**, 1718–1721 (2014).
31. E. R. Dohner, A. Jaffe, L. R. Bradshaw, H. I. Karunadasa, Intrinsic white-light emission from layered hybrid perovskites. *J. Am. Chem. Soc.* **136**, 13154–13157 (2014).
32. T. Hu, M. D. Smith, E. R. Dohner, M.-J. Sher, X. Wu, M. T. Trinh, A. Fisher, J. Corbett, X.-Y. Zhu, H. I. Karunadasa, A. M. Lindenberg, Mechanism for broadband white-light emission from two-dimensional (110) hybrid perovskites. *J. Phys. Chem. Lett.* **7**, 2258–2263 (2016).
33. M. Safdari, P. H. Svensson, M. T. Hoang, I. Oh, L. Kloo, J. M. Gardner, Layered 2D alkyldiammonium lead iodide perovskites: Synthesis, characterization, and use in solar cells. *J. Mater. Chem. A* **4**, 15638–15646 (2016).
34. T. Zhang, L. Xie, L. Chen, N. Guo, G. Li, Z. Tian, B. Mao, Y. Zhao, In situ fabrication of highly luminescent bifunctional amino acid crosslinked 2D/3D $NH_3C_4H_9COO(CH_3NH_3PbBr_3)_n$ perovskite films. *Adv. Funct. Mater.* **27**, 1603568 (2017).
35. V. D'Innocenzo, A. R. Srimath Kandada, M. De Bastiani, M. Gandini, A. Petrozza, Tuning the light emission properties by band gap engineering in hybrid lead halide perovskite. *J. Am. Chem. Soc.* **136**, 17730–17733 (2014).
36. M. Yang, Y. Zhou, Y. Zeng, C.-S. Jiang, N. P. Padture, K. Zhu, Square-centimeter solution-processed planar $CH_3NH_3PbI_3$ perovskite solar cells with efficiency exceeding 15%. *Adv. Mater.* **27**, 6363–6370 (2015).
37. X. Li, D. Bi, C. Yi, J.-D. Décoppet, J. Luo, S. M. Zakeeruddin, A. Hagfeldt, M. Grätzel, A vacuum flash–assisted solution process for high-efficiency large-area perovskite solar cells. *Science* **353**, 58–62 (2016).
38. D. H. Cao, C. C. Stoumpos, O. K. Farha, J. T. Hupp, M. G. Kanatzidis, 2D homologous perovskites as light-absorbing materials for solar cell applications. *J. Am. Chem. Soc.* **137**, 7843–7850 (2015).

Acknowledgments: We thank G. Jacopin for his help with the PL analysis. **Funding:** Y.Z. acknowledges the support of the National Natural Science Foundation of China (grant 51372151) and a Huoyingdong grant (151046). M.I.D. and M.G. acknowledge the King Abdulaziz City for Science and Technology and funding from the European Union's Horizon 2020 Programme, through a Future and Emerging Technologies (FET) Open research and innovation action under grant agreement no. 687008. **Author contributions:** Y.Z. and M.G. designed and directed the research. T.Z., M.I.D., G.L., N.G., and F.X. fabricated and characterized the perovskite thin films and devices. Y.Z., T.Z., M.I.D., and M.G. wrote the manuscript, with inputs from all authors. **Competing interests:** The authors declare that they have no competing interests. **Data and materials availability:** All data needed to evaluate the conclusions in the paper are present in the paper and/or in the Supplementary Materials. Additional data are available from Y.Z. (yixin.zhao@sjtu.edu.cn) upon request.

Submitted 19 March 2017
Accepted 11 September 2017
Published 29 September 2017
10.1126/sciadv.1700841

Citation: T. Zhang, M. I. Dar, G. Li, F. Xu, N. Guo, M. Grätzel, Y. Zhao, Bication lead iodide 2D perovskite component to stabilize inorganic α-$CsPbI_3$ perovskite phase for high-efficiency solar cells. *Sci. Adv.* **3**, e1700841 (2017).